The Journal of Chemical Physics

An enhanced sampling QM/AMOEBA approach: The case of the excited state intramolecular proton transfer in solvated 3-hydroxyflavone

Cite as: J. Chem. Phys. **154**, 184107 (2021); https://doi.org/10.1063/5.0046844
Submitted: 07 February 2021 . Accepted: 08 April 2021 . Published Online: 12 May 2021

Michele Nottoli, Mattia Bondanza, Filippo Lipparini, and Benedetta Mennucci

The Journal of Chemical Physics ARTICLE scitation.org/journal/jcp

An enhanced sampling QM/AMOEBA approach: The case of the excited state intramolecular proton transfer in solvated 3-hydroxyflavone

Cite as: J. Chem. Phys. 154, 184107 (2021); doi: 10.1063/5.0046844
Submitted: 7 February 2021 • Accepted: 8 April 2021 •
Published Online: 12 May 2021

Michele Nottoli,[a] Mattia Bondanza, Filippo Lipparini, and Benedetta Mennucci[b]

AFFILIATIONS

Dipartimento di Chimica e Chimica Industriale, Università di Pisa, Via G. Moruzzi 13, 56124 Pisa, Italy

Note: This paper is part of the JCP Special Collection in Honor of Women in Chemical Physics and Physical Chemistry.
[a] **Electronic mail:** michele.nottoli@phd.unipi.it
[b] **Author to whom correspondence should be addressed:** benedetta.mennucci@unipi.it

ABSTRACT

We present an extension of the polarizable quantum mechanical (QM)/AMOEBA approach to enhanced sampling techniques. This is achieved by connecting the enhanced sampling PLUMED library to the machinery based on the interface of Gaussian and Tinker to perform QM/AMOEBA molecular dynamics. As an application, we study the excited state intramolecular proton transfer of 3-hydroxyflavone in two solvents: methanol and methylcyclohexane. By using a combination of molecular dynamics and umbrella sampling, we find an ultrafast component of the transfer, which is common to the two solvents, and a much slower component, which is active in the protic solvent only. The mechanisms of the two components are explained in terms of intramolecular vibrational redistribution and intermolecular hydrogen-bonding, respectively. Ground and excited state free energies along an effective reaction coordinate are finally obtained allowing for a detailed analysis of the solvent mediated mechanism.

I. INTRODUCTION

In the last few years, there has been a significant progress in the use of hybrid approaches coupling quantum mechanical (QM) and classical models for describing dynamic processes of molecules in solution and more complex environments.[1–3] In most cases, a Molecular Mechanics (MM) force field has been used for the classical part of the system and an electrostatic embedding (EE) scheme for the coupling between the QM and the MM subsystems.[4–7]

EE-QM/MM molecular dynamics (MD) simulations have seen many successful applications in the study of ultrafast and fast processes (from hundreds of fs to few ps), especially when combined with inexpensive QM methods such as semiempirical methods.[8] However, their application to dynamic processes extending beyond the ps scale is still a challenge due to the overwhelming computational cost, especially if an *ab initio* QM method is used. Moreover, due to the EE scheme, it is not possible to account for the environment response to time-dependent (TD) changes in the electronic density of the embedded quantum subsystem. The latter limitation can be overcome by using a more sophisticated polarizable embedding,[9–12] which endows the MM atoms with the possibility to dynamically respond to changes in the QM charge distributions, thus making these approaches more suited to describe excited state (ES) processes.[3]

During the last decade, in our group, we have focused on the induced point dipole (IPD) formulation of polarizable embeddings.[13–23] In this framework, each atom in the MM subsystem bears a parameterized polarizability, which under the effect of the system's electric field produces an induced dipole, which, in turn, alters the system's electrostatics. We have developed a self-consistent approach that is able to variationally achieve mutual polarization for the MM induced electrostatics and the embedded quantum electron density, and we extended it to the treatment of excited states in the framework of linear response theory.[19,20,24,25] Recently, we pushed

forward the computational limits of this methodology by introducing a general linear scaling implementation based on the fast multipole method.[26–28] The efficiency of our implementation removes an important barrier that has previously limited the use of a polarizable QM/MM description, as the latter can be considerably more expensive than a EE treatment. However, the combination of linear scaling and fast convergence of the polarization equations makes the overhead introduced by the environment's polarization limited.[27,28] While the success of EE QM/MM is unquestionable, a polarizable description is more physically robust, especially when large and sudden changes in the QM density are observed. Reducing its computational cost thus paves the way to its systematic use for the study of photoinduced processes.

We have implemented our IPD model in a local version of the Gaussian software package;[29] currently, this implementation allows us to compute energies and analytical gradients, for ground-state [with HF, density functional theory (DFT), and MP2] and excited-state (TD-DFT) systems with up to several tens of thousands of atoms in the MM part.[28] In particular, our IPD model of choice is the Atomic Multipole Optimized Energetics for Biomolecular Applications (AMOEBA) force field.[30,31] AMOEBA is one of the most advanced force fields, but it also has a particularly complex electrostatic functional form (with static multipoles up to the quadrupoles and two independent sets of induced dipoles) that makes it more difficult to handle with respect to other polarizable force fields. The linear scaling formulation of IPD QM/MM embedding that we implemented in Gaussian is able to efficiently deal with all the features required by the AMOEBA force field.[28] The QM/AMOEBA approach has also been extended to ground and excited state Born–Oppenheimer molecular dynamics (BO-MD) by interfacing the Gaussian implementation with Tinker, which is the driver for the generation of the MD trajectory.[20,24,32]

Here, we make a further step ahead by presenting, for the first time, an excited state QM/AMOEBA MD in conjunction with enhanced sampling techniques. Enhanced sampling methods do not rely on any assumption on the underlying potential energy surface and are generally derived from thermodynamical and statistical considerations. As a consequence, their combination with QM/MM methods does not pose any theoretical issue. To perform such simulations, we coupled our setup, which is composed by Gaussian and Tinker as the MD driver, to PLUMED. The PLUMED package[33] is one of the most flexible and widely used software packages to perform enhanced sampling MD simulations; it implements many different methods and provides a simple and well documented interface that allows us to integrate it with virtually every MD engine.

The Tinker–Gaussian–PLUMED machinery is applied to the study of the excited state intramolecular proton transfer (ESIPT) in solvated 3-hydroxyflavone (3HF): upon photoexcitation of the ground state (GS) normal **N** form, the excited state undergoes proton transfer to yield the excited state tautomer **T** form (Scheme 1).

Various experimental studies have shown that both the steady state fluorescence and the time resolved properties strongly depend on the solvent.[34–38] More specifically, in hydrogen-bonding solvents, the emission from both **N** and **T** forms is observed, whereas in non-hydrogen-bonding solvents, only **T** fluorescence is observed. Moreover, time-resolved studies have shown that the ESIPT process is characterized by two components, a fast (several tens of femtoseconds) component and a slower (around 10 ps) component.[39–42] The former is consistently observed in all solvents, whereas the latter is prominent in hydrogen-bonding solvents.[39,41] In this work, we are interested in studying the effect of the solvent in the tuning of the time-dependent process. For this reason, we performed simulations in two very different solvents: a polar and protic one (methanol, MeOH) and an apolar one (methylcyclohexane, MCH). While the ultrafast component of the process can be simulated using excited state BO-MD as has already successfully been done using BO-MD combined to either a MM solvent and/or an implicit solvent,[43–50] the slow component happens on a timescale that would render the cost of the simulations prohibitive. This motivates us to couple our multiscale machinery with enhanced sampling techniques in order to achieve the description of slower processes at an accessible computational cost.

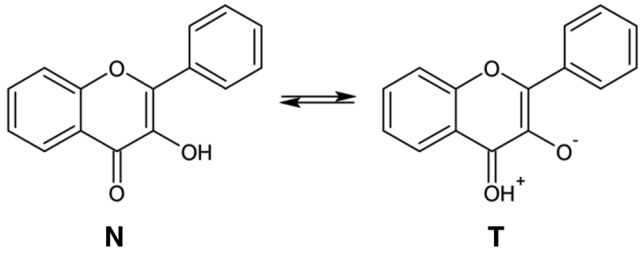

SCHEME 1. Scheme 1.

This paper is organized as follows: in Sec. II, we present the Tinker–Gaussian–PLUMED machinery and the computational details of the different techniques used. In Sec. III A, we discuss the results of the plain BO-MD and how they can be used to characterize the fast process. Finally, in Sec. III B, we present the results of the umbrella sampling (US) simulations, which has been used to characterize the slow component of the process.

II. METHODS

A. Tinker–Gaussian–PLUMED interface

In the last few years, we have developed an interface between Tinker[51,52] and Gaussian 16[29] packages for performing QM/AMOEBA MD simulations. Such an interface is particularly oriented to polarizable embedding, and it is optimized to run QM/AMOEBA MD simulations in ground and excited states.[24,53]

Here, we extended the integration to PLUMED to perform enhanced sampling simulations using a QM/AMOEBA Hamiltonian. PLUMED has a very simple mechanism that allows it to be interfaced with virtually every MD software. The main aim of the library is to compute user-defined functions of the system's configuration (generally called Collective Variable, CV) and use them to introduce bias forces in a controlled way, in order to enhance the sampling of the underlying potential energy surface. CVs are generally a complex combination of geometrical features of the system, which are able to provide a description of a complex process (such as a conformational change) in a reduced dimensional space.[54,55] From a practical point of view, the MD engine provides to the PLUMED library the geometry of the system, together with other information

about the simulation (namely, gradients, energy, masses, step number, and box dimensions); then, PLUMED combines these information according to the user's instructions, computes the bias forces, prints CV values on a log file, and gives back to the MD engine an updated version of the gradients in which the bias is already included.

A scheme of the interface is reported in Fig. 1. In our implementation, Tinker is the main driver of the MD simulation. Given a structure, it computes the bonded and van der Waals interactions; then, it assembles a QM/AMOEBA Gaussian input and calls Gaussian to run the QM/AMOEBA calculation. Once this is terminated, Tinker reads the Gaussian forces and energy and adds them to the already computed components. At this point, Tinker passes the structure and forces to the linked PLUMED library, which computes the collective variables and bias forces according to the user input. The bias forces are then passed back to Tinker, which finally performs the numerical integration to determine the following structure. All the communications between Tinker and Gaussian are performed through binary files, whereas the communication between Tinker and PLUMED is done directly in memory as PLUMED is a linked library.

B. Computational details

We used the AMOEBA force field for describing all the interactions in the solvent and the non-electrostatic interactions between the solute and the solvent. The solute was described with (TD) DFT using the ωB97XD functional[56] combined with the 6-31G(d, p) basis set where polarization functions have been used only for the O_N, O_T, and H atoms, which are directly involved in the ESIPT. The selection of a long-range corrected functional in combination with a 6-31G(d, p) basis set has been based on tests presented in a previous paper of some of the authors on absorption and emission energies of 3HF.[57] As a further test on the reliability of the selected QM level, we performed a relaxed scan of the geometry along the reaction coordinate described below: our combination of the basis set and functional gave an excited state barrier of 0.9 kcal/mol for the isolated system, which is in line with the estimate obtained by taking into account a tunneling mechanism 0.6–2.5 kcal/mol.[58]

Within the AMOEBA force field, the electrostatic and polarization interactions are represented in terms of a fixed multipolar expansion (up to quadrupoles) and an isotropic polarizability for the MM atoms. All the used MM parameters are those available in the AMOEBA parameterization for the two selected solvents, namely, methanol (MeOH) and methylcyclohexane (MCH).

For the simulations, we prepared two boxes containing 3HF in the two solvents. On these, we performed a two-step equilibration to prepare suitable starting conditions for the various analyses. The two steps are a standard MM dynamics run with the AMBER package[59] and a QM/AMOEBA dynamics run with Tinker, respectively.

For the AMBER MD in both solvents, we performed an initial geometry optimization followed by 50 ps of NVT heating from 0 to 50 K and by 1000 ps of NPT heating from 50 to 300 K. After that, 10 ns of NPT dynamics was performed at 300 K and standard pressure. The whole protocol uses an integration time step of 1 fs and the Generalized Amber force field (GAFF) to represent both the solute and the solvent. Simulations were run using periodic boundary conditions.

From the AMBER MD simulations, we selected 26 frames to be used as a starting point for the subsequent QM/AMOEBA simulations in each solvent. We selected drops containing the solute and all the solvent molecules within 30 Å from it (about 600 molecules of MCH and about 1800 molecules of MeOH). In the QM/MM MD simulations,[3] which are performed using localized basis functions for the QM subsystem, it is a natural choice to use non-periodic boundary conditions. Following the "droplet model" approach, a harmonic potential pointing toward the geometrical center of 3HF was applied to each solvent molecule that is further away than a certain distance.[60] The starting point of this boundary potential and its harmonic constant were selected to reproduce the experimental density of the solvent (more details are reported in the supplementary material).

For each of the configurations, we ran 5 ps long NVT equilibrations using the QM/AMOEBA Hamiltonian. The Langevin thermostat was used to keep the temperature at 300 K. This step was necessary to allow the system to relax on the new QM/AMOEBA potential energy surface. From these GS simulations, we extracted

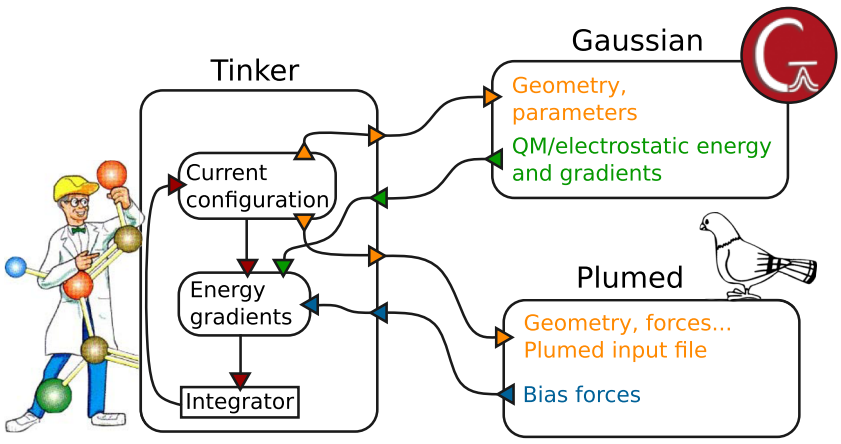

FIG. 1. A schematic representation of the Tinker–Gaussian–PLUMED interface. Tinker provides to Gaussian and PLUMED the coordinates of the system and other information (yellow arrows) to allow them to compute the QM/AMOEBA component of the forces (green arrows) and the bias forces, respectively (blue arrows). These components of the total gradient are summed together internally in Tinker and integrated in the MD cycle (red arrow).

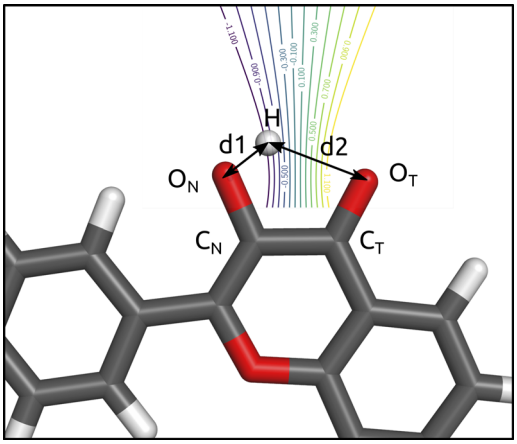

FIG. 2. Representation of the CV used to describe the ESIPT process. The CV is defined as the difference $d_1 - d_2$. Its value is negative in the **N** form and positive in the **T** form. Here, we plotted a series of contour lines of the CV from −1.1 (purple) to 1.1 (yellow).

the starting structures for both the plain excited state (ES) BO-MD and the umbrella sampling simulations.

In particular, we performed a series of 50 QM/AMOEBA BO-MD trajectories in the first excited state for each solvent. These simulations were run in the NVE ensemble; we performed 0.5 ps long trajectories, and we further extended 30 of them (for each solvent) up to 1.0 ps. The trajectories were finally analyzed using both the Python bindings to CPPTRAJ[61] and the MDAnalysis library.[62,63]

For the umbrella sampling (US) simulations, we defined a collective variable (CV). As an obvious choice, we selected the difference in the distance of H from the two oxygens; a schematic representation is given in Fig. 2. In this work, we refer to the oxygen in 3- (which is a hydroxyl oxygen in the **N** form of 3HF) as O_N and to the one in position 4- (which is a keto oxygen in the **N** form of 3HF) as O_T (see the scheme for the atom numbering). With this CV definition, the **N** form corresponds to a negative value of the CV, while the **T** form corresponds to the positive one; the transition point between the two states is at CV ≈ 0.

We performed a 2 ps long simulation on the ground and first excited states for 12 different values of the CV (−1.1, −0.9, −0.7, −0.5, −0.3, −0.1, 0.1, 0.3, 0.5, 0.7, 0.9, and 1.1) and for the two solvents mentioned above, for a total of 48 trajectories. The force constants used for the umbrella sampling potential are 29.0 kcal/mol $Å^{-2}$ for MCH and 34.0 kcal/mol $Å^{-2}$ for MeOH. These values were determined from the fluctuation of the CV on the GS, unbiased, trajectories. The configurations extracted from the US were analyzed with the Unbinned Weighted Histogram Analysis Method (UWHAM)/Multistate Bennett Acceptance Ratio (MBAR)[64,65] (using the FastMBAR implementation[66]) to reconstruct the free energy profile along the CV and the relative weights of the configuration extracted from the MD.

III. THE SIMULATION OF THE ESIPT PROCESS

Various experimental works studied the ESIPT process in different solvents.[39–42] In particular, a biexponential kinetics was found through pump–probe studies in polar and protic solvents with an ultra-fast femto-second component and a much slower (few picoseconds) component.[41] The latter component was explained with the breaking of solute–solvent hydrogen bonds prior to fast proton transfer, thus implying a diffusion controlled mechanism. In another study,[39] a similar biexponential process with an ~240 fs component and an ~10 ps component was also found in MCH, but it was imputed to the presence of hydrogen-bonding impurities in solution.

As regards the computational works, most of them focused on the simulation of the spectroscopic properties of the **N** and **T** tautomers and the involved PES.[42,57,67–69] An extensive investigation of the time-resolved process was, however, reported by Bellucci and Coker, using classical molecular dynamics in conjunction with empirical valence bond (EVB) potentials.[70] The goal of those simulations was the identification of the mechanisms responsible for both ultrafast transfer and slow proton transfer in different solvents. What they found is that the ultrafast process results from a combination of ballistic transfer and intramolecular vibrational redistribution, which leads to the excitation of a set of promoting modes. They also suggested that the slow proton transfer observed in protic solvents mainly results from strong intermolecular interactions that inhibit the process.

Here, we investigated two solvents, MCH and MeOH, as examples of an apolar and a polar protic solvent, respectively. Two different techniques have been used for the description of the ultra-fast and the slow components of the process: for the former, we used a swarm of plain BO-MD trajectories, whereas for the latter, we used umbrella sampling (US). US is a particularly effective technique when the slow degrees of freedom that are relevant for the process can be described with a single collective variable. US also offers a practical advantage: when the calculation of the potential energy surface cannot be massively parallelized across different nodes in a computer cluster, it allows us to trivially parallelize the whole calculation as each trajectory is completely independent of the others. The dimensionality of the problem and the degree of parallelization offered by different methods should be taken under serious consideration when planning a QM/MM enhanced sampling simulation: as a matter of fact, even if many methods are available within the proposed interface due to the low dimensionality of the ESIPT process and to the high computational cost of the QM/AMOEBA Hamiltonian, the use of US is perfectly suited to the needs of the process under analysis.

The results of the two sets of simulations are presented and discussed in Subsections III A and III B.

A. The ultrafast component

The ultrafast component of the process was studied using excited state BO-MD. Among the 50 trajectories generated for each solvent, we observed seven ESIPT events in MeOH and 26 ESIPT events in MCH. We defined the ESIPT transition as the moment at which the O_N–H and O_T–H distances are the same. The results of a reactive trajectory are shown in Fig. 3: a sudden jump in the ES–GS energy difference is observed together with the ESIPT event. Similar plots for all the 100 trajectories are given in the supplementary material.

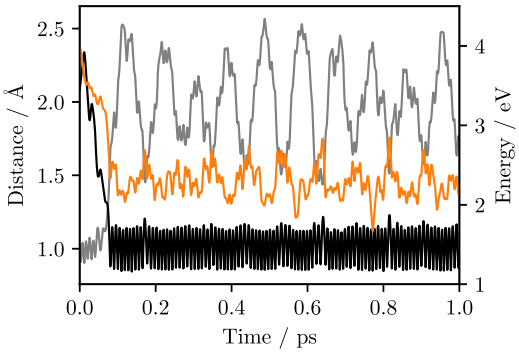

FIG. 3. Properties for an example MCH trajectory: Orange: ES–GS energy difference, black: O_T–H distance, and gray: O_N–H distance. The ESIPT occurs at 74 fs.

In Fig. 4, we provide a global view over the simulations, by reporting the fraction of reacted trajectories as a function of time. After 1 ps, these fractions are 67% in MCH and 17% in MeOH. Comparing these values with the results of Bellucci and Coker (66% and 50%, respectively),[70] we observe that the trend in MCH is exactly the same, whereas in MeOH, our calculations show a significantly smaller number of reactive events. We note that our results are, instead, in line with what experimentally observed.[39,41] Moreover, it clearly appears that in MeOH, the transfer occurs only in an ultrafast way (before 200 fs), while in MCH, longer times are also observed (within 0.8 ps). Given the number of generated trajectories, we cannot determine quantitative transfer times; however, the obtained picture qualitatively agrees with previous experimental and computational analyses.[39,41,70]

We also observe that, especially at short times, the ESIPT only occurs during specific time windows. This is a clear indication that there is a promoting vibrational mode, which is coherently stimulated upon excitation. The period measured between the first two time windows is about 90 fs, corresponding to the O_T–C_T–C_N–O_N in plane bending.[70] At longer times, this coherence is gradually lost and the time windows are no longer visible.

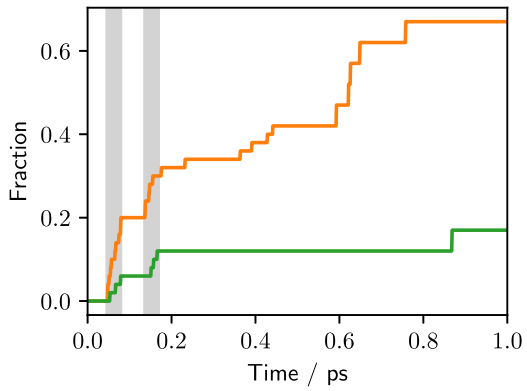

FIG. 4. Fraction of reacted trajectories as a function of time in MCH (orange) and MeOH (green). The first two windows at which the ESIPT takes place are shown in light gray. The fractions from 0.5 to 1.0 ps are normalized differently since they are computed on a subset of 20 trajectories.

In order to better understand the role of solute–solvent specific interactions, we performed a more detailed analysis on the presence of hydrogen bonds between 3HF and MeOH. There are three possible sites for intermolecular hydrogen bonds that are relevant to the process, involving the MeOH–O_T, MeOH–O_N, and MeHO–H pairs, respectively. Along both GS and ES trajectories, we estimated the presence of the aforementioned hydrogen bonds using two criteria, a distance condition (<3.0 Å) and an angle condition (>140°). All the results are reported in the supplementary material. The analysis shows that only the MeOH–O_T hydrogen bond is relevant for the ESIPT, as the other two are observed less frequently. Along the trajectories, we found that the MeOH–O_T bond is present on average in 18% of the configurations in the GS, 42% in the ES-**N** form, and is never present in the ES-**T** form. We also observed that all ESIPTs occur in 3HF molecules non-hydrogen bonded at O_T.

These findings provide some significant insights into the mechanism of the process. First, if a 3HF molecule has an O_T hydrogen bond in the GS, upon excitation, it will not undergo ESIPT in the investigated 1 ps time window. In other words, the lack of solute–solvent hydrogen bonds at the O_T site is a necessary condition for a fast ESIPT. Second, if a non-hydrogen bonded 3HF molecule does not undergo an early ESIPT (<250 fs), it will likely form a new O_T hydrogen bond, thus increasing the ESIPT energy barrier and preventing the reaction at the sub-picosecond scale. The second consideration explains the plateau observed in MeOH, and the two considerations together explain part of the different behavior experimentally observed in the two solvents.

As a last analysis, we searched for a further condition to rationalize which trajectories undergo an early ESIPT. This analysis is based on the continuous wavelet transform as proposed by Donati *et al.*[71] and successfully applied to the study of proton transfer processes in various systems.[44,46,50] For all the trajectories, we computed the difference in the distance of H from the two oxygens (see Fig. 2) and applied the wavelet transform to determine the coupled vibrations. For this analysis, we cropped all the trajectories to 0.5 ps to find consistent results. As a mother function, we used the complex Morlet wavelet,[72] which gives good results for vibrational signals.[50] The transform was performed using the PyWavelet library[73] (see also the supplementary material).

The wavelet transforms for all the trajectories are given in the supplementary material. Here, instead, we report two illustrative examples in MCH: a reactive one and a non-reactive one [see Figs. 5(a) and 5(b), respectively]. A qualitative interpretation of the two trajectories is performed connecting the frequencies of the features of the two wavelet transforms with the normal modes calculated for the **N** and **T** forms of 3HF through a standard harmonic model. Starting from the reactive trajectory [Fig. 5(a)], the high frequency region >3000 cm^{-1} (which corresponds to the O_N–H and O_T–H stretching) shows an apparent change in this signal after the ESIPT event. This change affects both the position and the intensity of the signal, which becomes blue-shifted and more intense; this is not surprising as we expect that upon ESIPT, a considerable amount of energy is transferred into this mode. In this region, the non-reactive trajectory shows only low-intensity signals in a frequency range roughly corresponding to the O_N–H stretch.

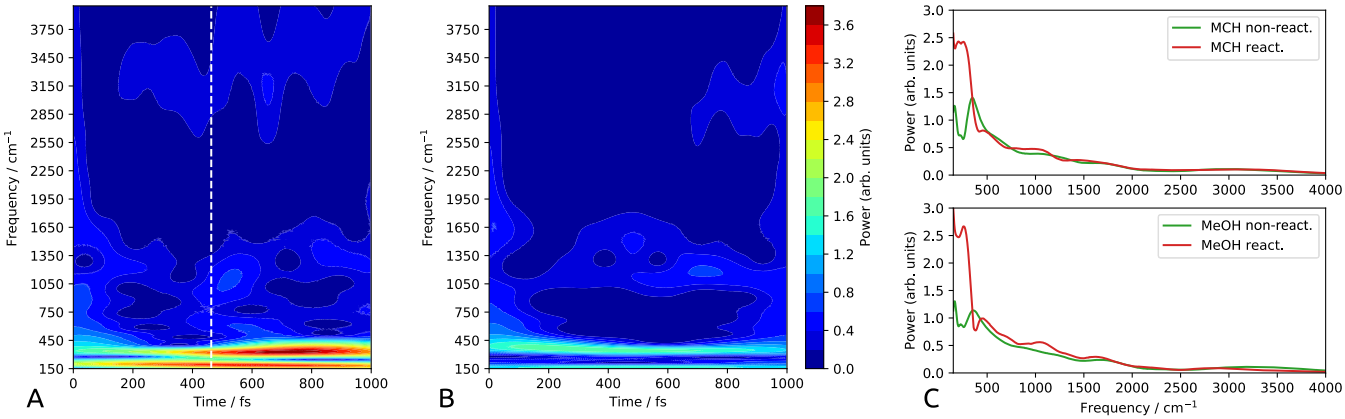

FIG. 5. (a) Wavelet transform for an example reactive trajectory in MCH. The power is represented with an arbitrary color scale. The time at which the ESIPT takes place is represented with the white dashed line. (b) Wavelet transform for an example non-reactive trajectory in MCH. (c) Average over the 25–50 fs time interval of the 2D wavelet transforms. Red: reacting trajectories, green: non-reacting trajectories, top: MCH, and bottom: MeOH. The same arbitrary power scale is used in (a), (b), and (c).

The region below 1600 cm^{-1} is the most interesting one. Here, we can distinguish two main signals: the first one, between 600 and 1600 cm^{-1}, can be ascribed to the C_N–C_T stretching and to other modes involving the C_N–O_N–H bending and the C_T–O_T–H bending, while the second in the region below 500 cm^{-1} is related to the already mentioned O_T–C_T–C_N–O_N in plane bending and other skeletal modes. While the first signal seems to be almost unaffected by the ESIPT, a large amount of energy is pushed in the second one upon the proton transfer. However, due to the time and frequency resolution provided by this wavelet analysis, it is difficult to assert whether the reactive trajectory has in its initial conditions a larger amount of energy in these modes.

To try to clarify this point, we computed the average of the 2D wavelet transforms over an initial time interval (between 25 and 50 fs) for the two types of trajectories and compared them. Such a time interval was chosen to avoid averaging any ESIPT process and to minimize the artifacts from the cone of influence of the wavelet transform.[74] The superimposed averages are shown in Fig. 5(c). The obtained data show that a trajectory that will lead to the proton transfer contains more energy in the modes with a frequency below 500 cm^{-1} and, even if much more weakly, with a frequency around ~1200 cm^{-1}.

By combining all the analyses, we confirm that the main promoting mode for the proton transfer is the O_T–C_T–C_N–O_N in plane bending, but we also observe that a reactive trajectory contains more energy in various modes in the low frequency region with respect to a non-reactive trajectory. This finding holds for both solvents and is consistent with the intramolecular vibrational redistribution mechanism proposed by Bellucci and Coker.[70]

B. The slow component

As a preliminary analysis for the investigation of the slow component, we checked if the selected CV (see Fig. 2) is the only relevant coordinate for the process. In particular, we investigated the role of the phenyl dihedral torsion, which previous works suggested as a relevant mode for the process.[39,75] To do so, we performed a 2D US simulation along the ESIPT CV and dihedral coordinates of 3HF in vacuum. The resulting free energy surfaces (FESs) for the GS and ES are reported in the supplementary material. From the calculated surfaces, we note that, in the GS, the **N** form has a larger rotational freedom around the dihedral angle with respect to the **T** one; the opposite is found in the ES where the **T** allows a larger out-of-plane torsion of the phenyl group. As a consequence, when the molecule is excited from the **N** form, the torsional potential suddenly increases and the system rapidly planarizes. This fast planarization upon excitation, also observed in the ES plain MD, is the only weak coupling between the two selected modes, and as such, we can conclude that the dihedral torsion does not significantly impact the transfer paths.

Once verified that the selected CV is the right one to follow, we applied US to the two solvents considered before. The simulation details are reported in Sec. II B. The trajectories were analyzed using UWHAM/MBAR to reconstruct the free energy profile along the CV and the relative weights of the configurations extracted from the MD.

We recall that within this framework, we have implicitly assumed that all the degrees of freedom are able to thermalize (in the limit of the sampling performed) at each value of the collective variable. This is somehow the opposite of the non-equilibrium picture provided by the previous analysis based on plain MD.

The resulting FESs [reported in Figs. 6(a) and 6(b)] present the expected inversion of the **N** and **T** basins going from ground to excited states in both solvents. To have a more quantitative analysis, in Table I, we report the free energy barriers for the direct (**N** → **T**) and inverse (**T** → **N**) reactions and the free energy difference between **N** and **T** forms in the ground and excited states.

As expected, the free energy barriers for the direct reaction calculated in the GS are very high (around 20 kcal mol^{-1}) in both solvents, and as such, they do not allow for the proton transfer at room temperature. Moving to the excited state, the barrier significantly decreases dropping below 5 kcal mol^{-1} for both solvents. However, the barrier in MeOH is about 2 kcal mol^{-1} higher than in

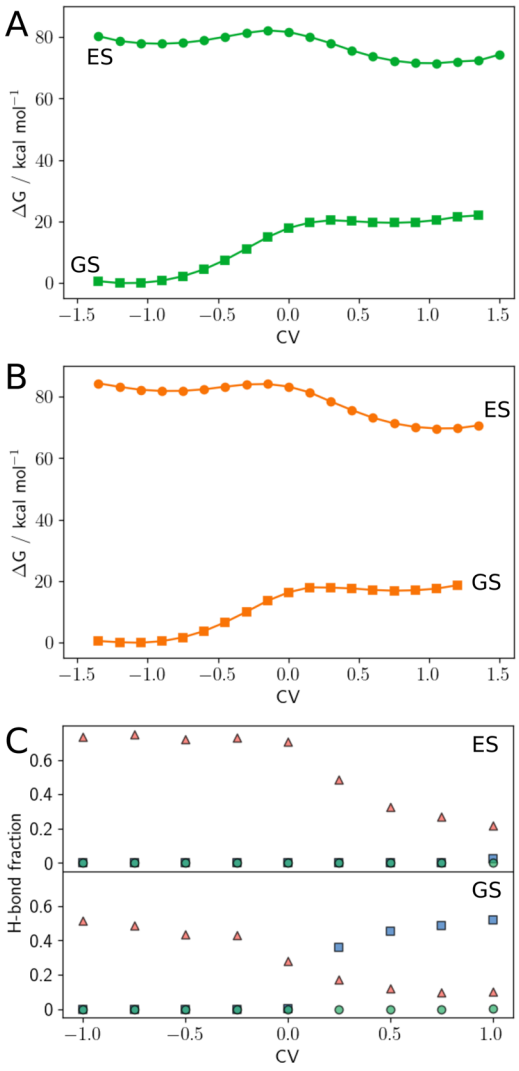

FIG. 6. Free energy surfaces of the ESIPT process in methanol (a) and in MCH (b) along the selected collective variable; for both solvents, the free energy profile (in kcal mol^{-1}) is reported for both ground (squares) and first excited states (circles). (c) Fraction of MeOH–O_T (red triangles), MeOH–O_N (blue squares), and MeHO–H (green circles) hydrogen bonds along the CV for ground state (GS) and excited state (ES).

MCH. This observation suggests a very different behavior in apolar aprotic solvents and in polar protic ones. In particular, by comparing the different free energy barriers and considering that the experimentally measured time constant for the slow ESIPT component in MeOH is 10 ps,[39] we can estimate that the slowest process observed in our US simulation in MCH has a time constant of about 300 fs. Here, we have assumed a comparable Arrhenius factor for the process in the two solvents. It is remarkable that this rough estimation of the transfer time is consistent with what found in Sec. III A. Our results therefore do not indicate a two component process for the ESIPT in MCH, but they describe a process with a very low barrier,

TABLE I. Free energy barriers for the direct and inverse reactions and the free energy difference between N and T forms in the ground and excited states. Energies are reported in kcal mol^{-1}.

Solvent	State	CV (**N**)	CV (**T**)	$\Delta G^{\ddagger}_{\mathbf{N}\to\mathbf{T}}$	$\Delta G^{\ddagger}_{\mathbf{T}\to\mathbf{N}}$	$\Delta G_{\mathbf{N}\to\mathbf{T}}$
MeOH	GS	1.2	−0.8	20.4	0.83	19.6
MeOH	ES	0.9	−1.1	4.35	10.7	−6.33
MCH	GS	1.0	−0.8	18.0	1.10	16.9
MCH	ES	0.9	−1.1	2.27	14.4	−12.2

which can be easily overcome at room temperature in the non-equilibrium state reached upon excitation. On the other hand, the picture provided by the US simulation for the ESIPT in MeOH is very different from what we have described in Sec. III A. This means that two distinct processes with two clearly different time rates are possible.

These differences between the two solvents can be explained as follows. Since MCH can only form very weak interactions with 3HF, it is not unexpected that its role in the reaction is very minor, if not null, regardless of an equilibrium or a nonequilibrium regime is assumed. On the other hand, the protic (and polar) character of MeOH is expected to significantly interact with the reactive part of the molecule. To verify this hypothesis, we have investigated the hydrogen bond fractions along the CV for both the GS and the ES. The results are shown in Fig. 6(c).

First, we note that in both electronic states, the fraction of MeHO–H hydrogen bonds is almost negligible along the whole reactive process. On the other hand, the hydrogen bonds with the two oxygen atoms of 3HF show clear trends. Considering the GS, we can clearly see that MeOH has a marked preference to form a MeOH–O_T hydrogen-bond in the **N** form (CV < 0) and a MeOH–O_N bond in the **T** form (CV > 0). These data suggest that the "initial state" (the ground state of the **N** form) has the O_T oxygen involved in a quite stable hydrogen bond with the solvent, consistently with what previously seen in plain GS MD. Upon excitation, this interaction becomes even stronger as confirmed by the increase in the MeOH–O_T hydrogen bond fraction: new MeOH–O_T hydrogen bonds are formed, and the already existing ones tighten. Considering the **T** form, we note an even sharper difference between the GS and the ES: while in the GS, a quite strong MeOH–O_N hydrogen bond is observed, this feature completely disappears in the ES. The two observations together can be explained in terms of a displacement of the ES electron density toward O_T independently of the position of the proton (see the supplementary material).

As shown in Sec. III A, the absence of a hydrogen bond between O_T and the solvent is necessary for the system to undergo an ultrafast ESIPT. Combining this observation with the complex behavior found for the hydrogen-bonding pattern in different electronic states and tautomeric forms, we can provide an insight about the atomistic origin of the slow and fast components of the ESIPT in MeOH.

In MCH, the ESIPT proceeds almost barrierless within few hundreds of fs. As a matter of fact, this is also what we have seen in the nonequilibrium simulations in MeOH as long as 3HF is not

involved in H-bonds with the solvent. The equilibrium picture provided by US, however, has revealed that the electronic excitation induces a strengthening of the MeOH–O_T hydrogen bond. When this interaction is present, the ESIPT process can only proceed through the hydrogen bond cleavage with a significant increase in the activation barrier. This slow process is what we observe from the analysis of the excited state FES in MeOH.

IV. CONCLUSIONS

We have presented an integration of three different software packages (Tinker, Gaussian, and PLUMED), which allows for extending QM/AMOEBA MD simulations on ground and excited states to relatively slow processes, thanks to the use of enhanced sampling techniques.

As a prototypical application, we reported the comparative study of the intramolecular proton transfer in excited 3HF in two different solvents: apolar and aprotic methylcyclohexane and polar and protic methanol. To investigate both fast (sub-ps) and slow components of the process, we combined two techniques. For the former, we used nonequilibrium MD trajectories obtained by vertically exciting the solute along its ground state dynamics. Instead, to investigate a possible slower component, we have used umbrella sampling simulations along a selected collective variable. The combination of these two techniques has shown a very different behavior of the ESIPT process in the two selected solvents in agreement with time-resolved measurements. In particular, an ultra-fast component (around 100–200 fs) is observed in both solvents but with a much lower probability in methanol. This component has been shown to proceed through an intramolecular vibrational redistribution mechanism, which is very similar in the two solvents. A second, much slower, component has been revealed by the US simulations in methanol. In fact, when the solute is involved in intermolecular hydrogen bonds, the ESIPT process can proceed only if such bonds are preliminarily broken. This requirement induces a significant increase in the free energy barrier with respect to MCH, thus explaining both the smaller probability for the ultrafast process and the appearance of a slow transfer process.

SUPPLEMENTARY MATERIAL

See the supplementary material for the details and benchmarks on the non-periodic boundary conditions used, technical details about the wavelet transform, the excitation energies and O_N–H and O_T–H distances along each ES plain trajectory, H-bonding analysis for each ES plain trajectory, wavelet transform for each ES plain trajectory, a graphical representation of the electron density difference between the excited and the ground states of 3HF in its **N** and **T** forms, and the free energy surfaces for the ground and excited states along the CV and the torsion of the phenyl group.

ACKNOWLEDGMENTS

M.B. and B.M. acknowledge funding from the European Research Council under Grant No. ERC-AdG-786714 (LIFETimeS).

DATA AVAILABILITY

The data that support the findings of this study are available within the article and its supplementary material.

REFERENCES

[1] E. Brunk and U. Rothlisberger, "Mixed quantum mechanical/molecular mechanical molecular dynamics simulations of biological systems in ground and electronically excited states," Chem. Rev. **115**, 6217–6263 (2015).
[2] E. Boulanger and J. N. Harvey, "QM/MM methods for free energies and photochemistry," Curr. Opin. Struct. Biol. **49**, 72–76 (2018).
[3] M. Bondanza, M. Nottoli, L. Cupellini, F. Lipparini, and B. Mennucci, "Polarizable embedding QM/MM: The future gold standard for complex (bio)systems?," Phys. Chem. Chem. Phys. **22**, 14433–14448 (2020).
[4] J. Gao, "Hybrid quantum and molecular mechanical simulations: An alternative avenue to solvent effects in organic chemistry," Acc. Chem. Res. **29**, 298–305 (1996).
[5] H. Lin and D. G. Truhlar, "QM/MM: What have we learned, where are we, and where do we go from here?," Theor. Chem. Acc. **117**, 185–199 (2006).
[6] H. M. Senn and W. Thiel, "QM/MM methods for biomolecular systems," Angew. Chem., Int. Ed. **48**, 1198–1229 (2009).
[7] M. W. van der Kamp and A. J. Mulholland, "Combined quantum mechanics/molecular mechanics (QM/MM) methods in computational enzymology," Biochemistry **52**, 2708–2728 (2013).
[8] W. Thiel, "Semiempirical quantum–chemical methods," Wiley Interdiscip. Rev.: Comput. Mol. Sci. **4**, 145–157 (2014).
[9] T. A. Halgren and W. Damm, "Polarizable force fields," Curr. Opin. Struct. Biol. **11**, 236–242 (2001).
[10] A. Warshel, M. Kato, and A. V. Pisliakov, "Polarizable force fields: History, test cases, and prospects," J. Chem. Theory Comput. **3**, 2034–2045 (2007).
[11] P. Cieplak, F.-Y. Dupradeau, Y. Duan, and J. Wang, "Polarization effects in molecular mechanical force fields," J. Phys.: Condens. Matter **21**, 333102–333122 (2009).
[12] Z. Jing, C. Liu, S. Y. Cheng, R. Qi, B. D. Walker, J.-P. Piquemal, and P. Ren, "Polarizable force fields for biomolecular simulations: Recent advances and applications," Annu. Rev. Biophys. **48**, 371–394 (2019).
[13] A. Warshel and M. Levitt, "Theoretical studies of enzymic reactions: Dielectric, electrostatic and steric stabilization of the carbonium ion in the reaction of lysozyme," J. Mol. Biol. **103**, 227–249 (1976).
[14] M. A. Thompson and G. K. Schenter, "Excited states of the bacteriochlorophyll b dimer of rhodopseudomonas viridis: A QM/MM study of the photosynthetic reaction center that includes MM polarization," J. Phys. Chem. **99**, 6374–6386 (1995).
[15] J. Gao, "Energy components of aqueous solution: Insight from hybrid QM/MM simulations using a polarizable solvent model," J. Comput. Chem. **18**, 1061–1071 (1997).
[16] P. T. van Duijnen and M. Swart, "Molecular and atomic polarizabilities: Thole's model revisited," J. Phys. Chem. A **102**, 2399 (1998).
[17] J. M. Olsen, K. Aidas, and J. Kongsted, "Excited states in solution through polarizable embedding," J. Chem. Theory Comput. **6**, 3721–3734 (2010).
[18] C. B. Nielsen, O. Christiansen, K. V. Mikkelsen, and J. Kongsted, "Density functional self-consistent quantum mechanics/molecular mechanics theory for linear and nonlinear molecular properties: Applications to solvated water and formaldehyde," J. Chem. Phys. **126**, 154112 (2007).
[19] C. Curutchet, A. Muñoz-Losa, S. Monti, J. Kongsted, G. D. Scholes, and B. Mennucci, "Electronic energy transfer in condensed phase studied by a polarizable QM/MM model," J. Chem. Theory Comput. **5**, 1838–1848 (2009).
[20] D. Loco, É. Polack, S. Caprasecca, L. Lagardère, F. Lipparini, J.-P. Piquemal, and B. Mennucci, "A QM/MM approach using the AMOEBA polarizable embedding: From ground state energies to electronic excitations," J. Chem. Theory Comput. **12**, 3654–3661 (2016).

[21]J. M. H. Olsen and J. Kongsted, in *Molecular Properties Through Polarizable Embedding*, Advances in Quantum Chemistry, edited by J. R. Sabin and E. Brändas (Elsevier, 2011), pp. 107–143.
[22]J. Dziedzic, Y. Mao, Y. Shao, J. Ponder, T. Head-Gordon, M. Head-Gordon, and C.-K. Skylaris, "TINKTEP: A fully self-consistent, mutually polarizable QM/MM approach based on the AMOEBA force field," J. Chem. Phys. **145**, 124106 (2016).
[23]X. Wu, J.-M. Teuler, F. Cailliez, C. Clavaguéra, D. R. Salahub, and A. de la Lande, "Simulating electron dynamics in polarizable environments," J. Chem. Theory Comput. **13**, 3985–4002 (2017).
[24]M. Nottoli, B. Mennucci, and F. Lipparini, "Excited state Born–Oppenheimer molecular dynamics through coupling between time dependent DFT and AMOEBA," Phys. Chem. Chem. Phys. **22**, 19532–19541 (2020).
[25]M. Nottoli and F. Lipparini, "General formulation of polarizable embedding models and of their coupling," J. Chem. Phys. **153**, 224108 (2020).
[26]L. Greengard and V. Rokhlin, "A fast algorithm for particle simulations," J. Comput. Phys. **73**, 325–348 (1987).
[27]S. Caprasecca, S. Jurinovich, L. Lagardère, B. Stamm, and F. Lipparini, "Achieving linear scaling in computational cost for a fully polarizable MM/continuum embedding," J. Chem. Theory Comput. **11**, 694–704 (2015).
[28]F. Lipparini, "General linear scaling implementation of polarizable embedding schemes," J. Chem. Theory Comput. **15**, 4312–4317 (2019).
[29]M. J. Frisch, G. W. Trucks, H. B. Schlegel, G. E. Scuseria, M. A. Robb, J. R. Cheeseman, G. Scalmani, V. Barone, G. A. Petersson, H. Nakatsuji, X. Li, M. Caricato, A. V. Marenich, J. Bloino, B. G. Janesko, R. Gomperts, B. Mennucci, H. P. Hratchian, J. V. Ortiz, A. F. Izmaylov, J. L. Sonnenberg, D. Williams-Young, F. Ding, F. Lipparini, F. Egidi, J. Goings, B. Peng, A. Petrone, T. Henderson, D. Ranasinghe, V. G. Zakrzewski, J. Gao, N. Rega, G. Zheng, W. Liang, M. Hada, M. Ehara, K. Toyota, R. Fukuda, J. Hasegawa, M. Ishida, T. Nakajima, Y. Honda, O. Kitao, H. Nakai, T. Vreven, K. Throssell, J. A. Montgomery, Jr., J. E. Peralta, F. Ogliaro, M. J. Bearpark, J. J. Heyd, E. N. Brothers, K. N. Kudin, V. N. Staroverov, T. A. Keith, R. Kobayashi, J. Normand, K. Raghavachari, A. P. Rendell, J. C. Burant, S. S. Iyengar, J. Tomasi, M. Cossi, J. M. Millam, M. Klene, C. Adamo, R. Cammi, J. W. Ochterski, R. L. Martin, K. Morokuma, O. Farkas, J. B. Foresman, and D. J. Fox, Gaussian 16, Revision A.03, Gaussian, Inc., Wallingford, CT, 2016.
[30]P. Ren and J. W. Ponder, "Polarizable atomic multipole water model for molecular mechanics simulation," J. Phys. Chem. B **107**, 5933–5947 (2003).
[31]Y. Shi, Z. Xia, J. Zhang, R. Best, C. Wu, J. W. Ponder, and P. Ren, "Polarizable atomic multipole-based AMOEBA force field for proteins," J. Chem. Theory Comput. **9**, 4046–4063 (2013).
[32]D. Loco, L. Lagardère, G. A. Cisneros, G. Scalmani, M. Frisch, F. Lipparini, B. Mennucci, and J.-P. Piquemal, "Towards large scale hybrid QM/MM dynamics of complex systems with advanced point dipole polarizable embeddings," Chem. Sci. **10**, 7200–7211 (2019).
[33]G. A. Tribello, M. Bonomi, D. Branduardi, C. Camilloni, and G. Bussi, "PLUMED 2: New feathers for an old bird," Comput. Phys. Commun. **185**, 604–613 (2014).
[34]P. K. Sengupta and M. Kasha, "Excited state proton-transfer spectroscopy of 3-hydroxyflavone and quercetin," Chem. Phys. Lett. **68**, 382–385 (1979).
[35]D. McMorrow and M. Kasha, "Intramolecular excited-state proton transfer in 3-hydroxyflavone. Hydrogen-bonding solvent perturbations," J. Phys. Chem. **88**, 2235–2243 (1984).
[36]V. I. Tomin, "Proton transfer reactions in the excited electronic state," in *Hydrogen Bonding and Transfer in the Excited State*, edited by K.-L. Han and G.-J. Zhao (John Wiley & Sons, Ltd., Chichester, UK, 2010), pp. 463–523.
[37]S. Protti and A. Mezzetti, "Solvent effects on the photophysics and photoreactivity of 3-hydroxyflavone: A combined spectroscopic and kinetic study," J. Mol. Liq. **205**, 110–114 (2015).
[38]T. Kumpulainen, B. Lang, A. Rosspeintner, and E. Vauthey, "Ultrafast elementary photochemical processes of organic molecules in liquid solution," Chem. Rev. **117**, 10826–10939 (2017).
[39]B. J. Schwartz, L. A. Peteanu, and C. B. Harris, "Direct observation of fast proton transfer: Femtosecond photophysics of 3-hydroxyflavone," J. Phys. Chem. **96**, 3591–3598 (1992).
[40]S. M. Ormson, D. LeGourrierec, R. G. Brown, and P. Foggi, "Sub-picosecond pump-probe spectroscopy of ESIPT in 3-hydroxyflavone," J. Chem. Soc., Chem. Commun. **1995**, 2133.
[41]S. Ameer-Beg, S. M. Ormson, R. G. Brown, P. Matousek, M. Towrie, E. T. J. Nibbering, P. Foggi, and F. V. R. Neuwahl, "Ultrafast measurements of excited state intramolecular proton transfer (ESIPT) in room temperature solutions of 3-hydroxyflavone and derivatives," J. Phys. Chem. A **105**, 3709–3718 (2001).
[42]K. Chevalier, M. M. N. Wolf, A. Funk, M. Andres, M. Gerhards, and R. Diller, "Transient IR spectroscopy and *ab initio* calculations on ESIPT in 3-hydroxyflavone solvated in acetonitrile," Phys. Chem. Chem. Phys. **14**, 15007 (2012).
[43]N. Kungwan, F. Plasser, A. J. A. Aquino, M. Barbatti, P. Wolschann, and H. Lischka, "The effect of hydrogen bonding on the excited-state proton transfer in 2-(2′-hydroxyphenyl)benzothiazole: A TDDFT molecular dynamics study," Phys. Chem. Chem. Phys. **14**, 9016 (2012).
[44]A. Petrone, G. Donati, P. Caruso, and N. Rega, "Understanding THz and IR signals beneath time-resolved fluorescence from excited-state ab initio dynamics," J. Am. Chem. Soc. **136**, 14866–14874 (2014).
[45]A. Petrone, D. B. Lingerfelt, D. B. Williams-Young, and X. Li, "Ab initio transient vibrational spectral analysis," J. Phys. Chem. Lett. **7**, 4501–4508 (2016).
[46]M. G. Chiariello, G. Donati, and N. Rega, "Time-resolved vibrational analysis of excited state ab initio molecular dynamics to understand photorelaxation: The case of the pyranine photoacid in aqueous solution," J. Chem. Theory Comput. **16**, 6007–6013 (2020).
[47]J. J. Goings and S. Hammes-Schiffer, "Nonequilibrium dynamics of proton-coupled electron transfer in proton wires: Concerted but asynchronous mechanisms," ACS Cent. Sci. **6**, 1594–1601 (2020).
[48]E. Odella, S. J. Mora, B. L. Wadsworth, J. J. Goings, M. A. Gervaldo, L. E. Sereno, T. L. Groy, D. Gust, T. A. Moore, G. F. Moore, S. Hammes-Schiffer, and A. L. Moore, "Proton-coupled electron transfer across benzimidazole bridges in bioinspired proton wires," Chem. Sci. **11**, 3820–3828 (2020).
[49]U. Raucci, M. G. Chiariello, and N. Rega, "Modeling excited-state proton transfer to solvent: A dynamics study of a super photoacid with a hybrid implicit/explicit solvent model," J. Chem. Theory Comput. **16**, 7033–7043 (2020).
[50]G. Donati, A. Petrone, and N. Rega, "Multiresolution continuous wavelet transform for studying coupled solute–solvent vibrations via *ab initio* molecular dynamics," Phys. Chem. Chem. Phys. **22**, 22645–22661 (2020).
[51]J. A. Rackers, Z. Wang, C. Lu, M. L. Laury, L. Lagardère, M. J. Schnieders, J.-P. Piquemal, P. Ren, and J. W. Ponder, "Tinker 8: Software tools for molecular design," J. Chem. Theory Comput. **14**, 5273–5289 (2018).
[52]L. Lagardère, L.-H. Jolly, F. Lipparini, F. Aviat, B. Stamm, Z. F. Jing, M. Harger, H. Torabifard, G. A. Cisneros, M. J. Schnieders, N. Gresh, Y. Maday, P. Y. Ren, J. W. Ponder, and J.-P. Piquemal, "Tinker-HP: A massively parallel molecular dynamics package for multiscale simulations of large complex systems with advanced point dipole polarizable force fields," Chem. Sci. **9**, 956–972 (2018).
[53]D. Loco, L. Lagardère, S. Caprasecca, F. Lipparini, B. Mennucci, and J.-P. Piquemal, "Hybrid QM/MM molecular dynamics with AMOEBA polarizable embedding," J. Chem. Theory Comput. **13**, 4025–4033 (2017).
[54]C. Abrams and G. Bussi, "Enhanced sampling in molecular dynamics using metadynamics, replica-exchange, and temperature-acceleration," Entropy **16**, 163–199 (2013).
[55]M. Bonomi, D. Branduardi, G. Bussi, C. Camilloni, D. Provasi, P. Raiteri, D. Donadio, F. Marinelli, F. Pietrucci, R. A. Broglia, and M. Parrinello, "PLUMED: A portable plugin for free-energy calculations with molecular dynamics," Comput. Phys. Commun. **180**, 1961–1972 (2009).
[56]J.-D. Chai and M. Head-Gordon, "Long-range corrected hybrid density functionals with damped atom–atom dispersion corrections," Phys. Chem. Chem. Phys. **10**, 6615 (2008).
[57]D. Loco, N. Gelfand, S. Jurinovich, S. Protti, A. Mezzetti, and B. Mennucci, "Polarizable QM/classical approaches for the modeling of solvation effects on UV–Vis and fluorescence spectra: An integrated strategy," J. Phys. Chem. A **122**, 390–397 (2018).
[58]A. N. Bader, V. G. Pivovarenko, A. P. Demchenko, F. Ariese, and C. Gooijer, "Excited state and ground state proton transfer rates of 3-hydroxyflavone and its

derivatives studied by Shpol'skii spectroscopy: The influence of redistribution of electron density," J. Chem. Phys. B **108**, 10589–10595 (2004).
[59]D. A. Case, I. Y. Ben-Shalom, S. R. Brozell, D. S. Cerutti, T. E. Cheatham III, V. W. D. Cruzeiro, T. A. Darden, R. E. Duke, D. Ghoreishi, M. K. Gilson, H. Gohlke, A. W. Goetz, D. Greene, R. Harris, N. Homeyer, S. Izadi, A. Kovalenko, T. Kurtzman, T. S. Lee, S. LeGrand, P. Li, C. Lin, J. Liu, T. Luchko, R. Luo, D. J. Mermelstein, K. M. Merz, Y. Miao, G. Monard, C. Nguyen, H. Nguyen, I. Omelyan, A. Onufriev, F. Pan, R. Qi, D. R. Roe, A. Roitberg, C. Sagui, S. Schott-Verdugo, J. Shen, C. L. Simmerling, J. Smith, R. Salomon-Ferrer, J. Swails, R. C. Walker, J. Wang, H. Wei, R. M. Wolf, X. Wu, L. Xiao, D. M. York, and P. A. Kollman, Amber 2018, 2018.
[60]T. Vasilevskaya and W. Thiel, "Periodic boundary conditions in QM/MM calculations: Implementation and tests," J. Chem. Theory Comput. **12**, 3561–3570 (2016).
[61]D. R. Roe and T. E. Cheatham, "PTRAJ and CPPTRAJ: Software for processing and analysis of molecular dynamics trajectory data," J. Chem. Theory Comput. **9**, 3084–3095 (2013).
[62]R. Gowers, M. Linke, J. Barnoud, T. Reddy, M. Melo, S. Seyler, J. Domański, D. Dotson, S. Buchoux, I. Kenney, and O. Beckstein, "MDAnalysis: A python package for the rapid analysis of molecular dynamics simulations," in *Proceedings of the 15th Python in Science Conference* (SciPy, 2016).
[63]N. Michaud-Agrawal, E. J. Denning, T. B. Woolf, and O. Beckstein, "MDAnalysis: A toolkit for the analysis of molecular dynamics simulations," J. Comput. Chem. **32**, 2319–2327 (2011).
[64]Z. Tan, E. Gallicchio, M. Lapelosa, and R. M. Levy, "Theory of binless multi-state free energy estimation with applications to protein-ligand binding," J. Chem. Phys. **136**, 144102 (2012).
[65]M. R. Shirts and J. D. Chodera, "Statistically optimal analysis of samples from multiple equilibrium states," J. Chem. Phys. **129**, 124105 (2008).
[66]X. Ding, J. Z. Vilseck, and C. L. Brooks, "Fast solver for large scale multi-state Bennett acceptance ratio equations," J. Chem. Theory Comput. **15**, 799–802 (2019).
[67]A. Mühlpfordt, T. Bultmann, N. P. Ernsting, and B. Dick, "Excited-state intramolecular proton transfer in jet-cooled 3-hydroxyflavone. Deuteration studies, vibronic double-resonance experiments, and semiempirical (AM1) calculations of potential-energy surfaces," Chem. Phys. **181**, 447–460 (1994).
[68]R. Casadesús, O. Vendrell, M. Moreno, J. M. Lluch, and K. Morokuma, "On the intramolecular proton transfer of 3-hydroxyflavone in the first singlet excited state: A theoretical study," Chem. Phys. **325**, 243–250 (2006).
[69]S. Höfener, P. C. Kooijman, J. Groen, F. Ariese, and L. Visscher, "Fluorescence behavior of (selected) flavonols: A combined experimental and computational study," Phys. Chem. Chem. Phys. **15**, 12572 (2013).
[70]M. A. Bellucci and D. F. Coker, "Molecular dynamics of excited state intramolecular proton transfer: 3-hydroxyflavone in solution," J. Chem. Phys. **136**, 194505 (2012).
[71]G. Donati, A. Petrone, P. Caruso, and N. Rega, "The mechanism of a green fluorescent protein proton shuttle unveiled in the time-resolved frequency domain by excited state *ab initio* dynamics," Chem. Sci. **9**, 1126–1135 (2018).
[72]A. Grossmann and J. Morlet, "Decomposition of hardy functions into square integrable wavelets of constant shape," SIAM J. Math. Anal. **15**, 723–736 (1984).
[73]G. Lee, R. Gommers, F. Waselewski, K. Wohlfahrt, and A. O'Leary, "PyWavelets: A python package for wavelet analysis," J. Open Source Software **4**, 1237 (2019).
[74]C. Torrence and G. P. Compo, "A practical guide to wavelet analysis," Bull. Am. Meteorol. Soc. **79**, 61–78 (1998).
[75]M. Itoh, K. Tokumura, Y. Tanimoto, Y. Okada, H. Takeuchi, K. Obi, and I. Tanaka, "Time-resolved and steady-state fluorescence studies of the excited-state proton transfer in 3-hydroxyflavone and 3-hydroxychromone," J. Am. Chem. Soc. **104**, 4146–4150 (1982).